

1 **MitoChime: A Machine Learning Pipeline for**
2 **Detecting PCR-Induced Chimeras in**
3 **Mitochondrial Illumina Reads**

4 A Special Project Proposal
5 Presented to
6 the Faculty of the Division of Physical Sciences and Mathematics
7 College of Arts and Sciences
8 University of the Philippines Visayas
9 Miagao, Iloilo

10 In Partial Fulfillment
11 of the Requirements for the Degree of
12 Bachelor of Science in Computer Science

13 by

14 Duranne Duran
15 Yvonne Lin
16 Daniella Pailden

17 Adviser
18 Francis D. Dimzon, Ph.D.

19 December 30, 2025

Abstract

21 Next-generation sequencing (NGS) platforms have advanced research but re-
22 main susceptible to artifacts such as PCR-induced chimeras that compromise
23 mitochondrial genome assembly. These artificial hybrid sequences are prob-
24 lematic for small, circular, and repetitive mitochondrial genomes, where they
25 can generate fragmented contigs and false junctions. Existing detection tools,
26 such as UCHIME, are optimized for amplicon-based microbial community ana-
27 lysis and depend on reference databases or abundance assumptions unsuitable
28 for organellar assembly. To address this gap, this study presents MitoChime,
29 a machine learning pipeline for detecting PCR-induced chimeric reads in *Sar-*
30 *dinella lemuru* Illumina paired-end data without relying on external reference
31 databases.

32 Using simulated datasets containing clean and chimeric reads, a feature
33 set was extracted, combining alignment-based metrics (e.g., supplementary
34 alignments, soft-clipping) with sequence-derived statistics (e.g., k-mer com-
35 position, microhomology). A comparative evaluation of supervised learning
36 models identified tree-based ensembles CatBoost and Gradient Boosting as top
37 performers, achieving an F1-score of 0.77 and an ROC-AUC of 0.84 on held-
38 out test data. Feature importance analysis highlighted soft-clipping and k-mer
39 compositional shifts as the strongest predictors of chimerism, whereas micro-
40 homology contributed minimally. Integrating MitoChime as a pre-assembly
41 step can aid in streamlining mitochondrial reconstruction pipelines.

42 **Keywords:** Chimera detection, Mitochondrial genome,
Assembly, Machine learning

⁴³ **Contents**

⁴⁴	1 Introduction	1
⁴⁵	1.1 Overview	1
⁴⁶	1.2 Problem Statement	3
⁴⁷	1.3 Research Objectives	3
⁴⁸	1.3.1 General Objective	3
⁴⁹	1.3.2 Specific Objectives	4
⁵⁰	1.4 Scope and Limitations of the Research	4
⁵¹	1.5 Significance of the Research	6
⁵²	2 Review of Related Literature	7
⁵³	2.1 The Mitochondrial Genome	7
⁵⁴	2.1.1 Mitochondrial Genome Assembly	8

55	2.2 PCR Amplification and Chimera Formation	9
56	2.3 Existing Traditional Approaches for Chimera Detection	10
57	2.3.1 UCHIME	11
58	2.3.2 UCHIME2	12
59	2.3.3 CATch	13
60	2.3.4 ChimPipe	14
61	2.4 Machine Learning Approaches for Chimera and Sequence Quality	
62	Detection	15
63	2.4.1 Feature-Based Representations of Genomic Sequences . . .	15
64	2.5 Synthesis of Chimera Detection Approaches	16
65	3 Research Methodology	19
66	3.1 Research Activities	19
67	3.1.1 Data Collection	20
68	3.1.2 Feature Extraction Pipeline	23
69	3.1.3 Machine Learning Model Development	26
70	3.1.4 Model Benchmarking, Hyperparameter Optimization, and	
71	Evaluation	27
72	3.1.5 Feature Importance, Feature Selection, and Interpretation	29

73	3.1.6 Validation and Testing	31
74	3.1.7 Documentation	32
75	3.2 Calendar of Activities	32
76	4 Results and Discussion	34
77	4.1 Descriptive Analysis of Features	34
78	4.1.1 Exploratory Data Analysis	35
79	4.2 Baseline Classification Performance	36
80	4.3 Effect of Hyperparameter Tuning	38
81	4.4 Detailed Evaluation of Representative Models	39
82	4.4.1 Confusion Matrices and Error Patterns	40
83	4.4.2 ROC and Precision–Recall Curves	41
84	4.5 Feature Importance	42
85	4.5.1 Permutation Importance of Individual Features	42
86	4.5.2 Feature Family Importance	44
87	4.6 Summary of Findings	46
88	A Exploratory Data Analysis	48
89	A.1 Histograms of Key Features	48

⁹⁰ List of Figures

⁹¹	3.1 Process diagram of the study workflow.	20
⁹²	4.1 Feature correlation heatmap showing relationships among alignment-derived and sequence-derived features.	36
⁹³		
⁹⁴	4.2 Test F1 of all baseline classifiers, showing that no single model clearly dominates and several achieve comparable performance. . .	37
⁹⁵		
⁹⁶	4.3 Comparison of test F1 (left) and ROC–AUC (right) for baseline and tuned models.	39
⁹⁷		
⁹⁸	4.4 Confusion matrices for the four representative models on the held-out test set.	41
⁹⁹		
¹⁰⁰	4.5 ROC (left) and precision–recall (right) curves for the four representative models on the held-out test set.	42
¹⁰¹		
¹⁰²	4.6 Permutation-based feature importance for four representative classifiers.	44
¹⁰³		
¹⁰⁴	4.7 Aggregated feature family importance across four models.	46

107 List of Tables

₁₁₂ **Chapter 1**

₁₁₃ **Introduction**

₁₁₄ **1.1 Overview**

₁₁₅ The rapid advancement of next-generation sequencing (NGS) technologies has
₁₁₆ transformed genomic research by enabling high-throughput and cost-effective
₁₁₇ DNA analysis (Metzker, 2010). Among current platforms, Illumina sequencing
₁₁₈ remains the most widely adopted, capable of producing millions of short reads
₁₁₉ that can be assembled into reference genomes or analyzed for genetic variation
₁₂₀ (Bentley et al., 2008; Glenn, 2011). Despite its high base-calling accuracy,
₁₂₁ Illumina sequencing is prone to artifacts introduced during library preparation,
₁₂₂ particularly polymerase chain reaction (PCR)-induced chimeras, which are ar-
₁₂₃ tificial hybrid sequences that do not exist in the true genome (Judo, Wedel, &
₁₂₄ Wilson, 1998).

₁₂₅ PCR chimeras form when incomplete extension products from one template

anneal to an unrelated DNA fragment and are extended, creating recombinant reads (Qiu et al., 2001). In mitochondrial genome assembly, such artifacts are especially problematic because the mitochondrial genome is small, circular, and often repetitive (Boore, 1999; Cameron, 2014). Even a small number of chimeric or misjoined reads can reduce assembly contiguity and introduce false junctions during organelle genome reconstruction (Dierckxsens, Mardulyn, & Smits, 2017; Hahn, Bachmann, & Chevreux, 2013; Jin et al., 2020). Existing assembly tools such as GetOrganelle and MITObim assume that input reads are largely free of such artifacts (Hahn et al., 2013; Jin et al., 2020). Consequently, undetected chimeras may produce fragmented assemblies or misidentified organellar boundaries. To ensure accurate reconstruction of mitochondrial genomes, a reliable method for detecting PCR-induced chimeras before assembly is essential.

This study focuses on mitochondrial sequencing data from the genus *Sardinella*, a group of small pelagic fishes widely distributed in Philippine waters. Among them, *Sardinella lemuru* (Bali sardinella) is one of the country's most abundant and economically important species, providing protein and livelihood to coastal communities (Labrador, Agmata, Palermo, Ravago-Gotanco, & Pante, 2021; Willette, Bognot, Mutia, & Santos, 2011). Accurate mitochondrial assemblies are critical for understanding its population genetics, stock structure, and evolutionary history. However, assembly pipelines often encounter errors or fail to complete due to undetected chimeric reads. To address this gap, this research introduces MitoChime, a machine learning pipeline designed to detect PCR-induced chimeric reads using both alignment-based and sequence-derived statistical features. The tool aims to provide bioinformatics laboratories, particularly the Philippine Genome Center Visayas (PGC Visayas), with an efficient

151 solution for improving mitochondrial genome reconstruction.

152 1.2 Problem Statement

153 Chimeric reads can distort assembly graphs and cause misassemblies, with par-
154 ticularly severe effects in mitochondrial genomes (Boore, 1999; Cameron, 2014).
155 Existing assembly pipelines such as GetOrganelle, MITObim, and NOVOPlasty
156 assume that sequencing reads are free of such artifacts (Dierckxsens et al., 2017;
157 Hahn et al., 2013; Jin et al., 2020). At PGC Visayas, several mitochondrial as-
158 semblies have failed or yielded incomplete contigs despite sufficient coverage, sug-
159 gesting that undetected chimeric reads compromise assembly reliability. Mean-
160 while, existing chimera detection tools such as UCHIME and VSEARCH were
161 developed primarily for amplicon-based community analysis and rely heavily on
162 reference or taxonomic comparisons (Edgar, Haas, Clemente, Quince, & Knight,
163 2011; Rognes, Flouri, Nichols, Quince, & Mahé, 2016). These approaches are un-
164 suitable for single-species organellar data, where complete reference genomes are
165 often unavailable.

166 1.3 Research Objectives

167 1.3.1 General Objective

168 This study aims to develop and evaluate a machine learning-based pipeline (Mi-
169 toChime) that detects PCR-induced chimeric reads in *Sardinella lemuru* mito-

₁₇₀ chondrial sequencing data in order to improve the quality and reliability of down-
₁₇₁ stream mitochondrial genome assemblies.

₁₇₂ 1.3.2 Specific Objectives

₁₇₃ Specifically, the study aims to:

- ₁₇₄ 1. construct simulated *Sardinella lemuru* Illumina paired-end datasets contain-
₁₇₅ ing both clean and PCR-induced chimeric reads,
- ₁₇₆ 2. extract alignment-based and sequence-based features such as k-mer compo-
₁₇₇ sition, junction complexity, and split-alignment counts from both clean and
₁₇₈ chimeric reads,
- ₁₇₉ 3. train, validate, and compare supervised machine learning models for classi-
₁₈₀ fying reads as clean or chimeric,
- ₁₈₁ 4. determine feature importance and identify indicators of PCR-induced
₁₈₂ chimerism,
- ₁₈₃ 5. integrate the optimized classifier into a modular and interpretable pipeline
₁₈₄ deployable on standard computing environments at PGC Visayas.

₁₈₅ 1.4 Scope and Limitations of the Research

₁₈₆ This study focuses solely on PCR-induced chimeric reads in *Sardinella lemuru*
₁₈₇ mitochondrial sequencing data, with the species choice guided by four consid-
₁₈₈ erations: (1) to limit interspecific variation in mitochondrial genome size, GC

189 content, and repetitive regions so that differences in read patterns can be at-
190 tributed more directly to PCR-induced chimerism, (2) to align the analysis with
191 relevant *S. lemuru* sequencing projects at PGC Visayas, (3) to take advantage of
192 the availability of *S. lemuru* mitochondrial assemblies and raw datasets in public
193 repositories such as the National Center for Biotechnology Information (NCBI),
194 which facilitates reference selection and benchmarking, and (4) to develop a tool
195 that directly supports local studies on *S. lemuru* population structure and fisheries
196 management.

197 The study emphasizes `wgsim`-based simulations and selected empirical mito-
198 chondrial datasets from *S. lemuru*. It excludes naturally occurring chimeras, nu-
199 clear mitochondrial pseudogenes (NUMTs), and large-scale assembly rearrange-
200 ments in nuclear genomes. Feature extraction is restricted to low-dimensional
201 alignment and sequence statistics, such as k-mer frequency profiles, GC con-
202 tent, soft and hard clipping metrics, and split-alignment counts rather than high-
203 dimensional deep learning embeddings. This design keeps model behaviour inter-
204 pretable and ensures that the pipeline can be run on standard workstations at
205 PGC Visayas. Testing on long-read platforms (e.g., Nanopore, PacBio) and other
206 taxa is outside the scope of this project.

207 Other limitations in this study include the following: simulations with vary-
208 ing error rates were not performed, so the effect of different sequencing errors on
209 model performance remains unexplored; alternative parameter settings, including
210 k-mer lengths and microhomology window sizes, were not systematically tested,
211 which could affect the sensitivity of both k-mer and microhomology feature de-
212 tection; and the machine learning models rely on supervised training with labeled
213 examples, which may limit their ability to detect novel or unexpected chimeric

214 patterns.

215 1.5 Significance of the Research

216 This research provides both methodological and practical contributions to mito-
217 chondrial genomics and bioinformatics. First, MitoChime detects PCR-induced
218 chimeric reads prior to genome assembly, with the goal of improving the con-
219 tiguity and correctness of *Sardinella lemuru* mitochondrial assemblies. Second,
220 it replaces informal manual curation with a documented workflow, improving au-
221 tomation and reproducibility. Third, the pipeline is designed to run on computing
222 infrastructures commonly available in regional laboratories, enabling routine use
223 at facilities such as PGC Visayas. Finally, more reliable mitochondrial assemblies
224 for *S. lemuru* provide a stronger basis for downstream applications in the field of
225 fisheries and genomics.

²²⁶ **Chapter 2**

²²⁷ **Review of Related Literature**

²²⁸ This chapter presents an overview of the literature relevant to the study. It
²²⁹ discusses the biological and computational foundations underlying mitochondrial
²³⁰ genome analysis and assembly, as well as existing tools, algorithms, and techniques
²³¹ related to chimera detection and genome quality assessment. The chapter aims to
²³² highlight the strengths, limitations, and research gaps in current approaches that
²³³ motivate the development of the present study.

²³⁴ **2.1 The Mitochondrial Genome**

²³⁵ Mitochondrial genome (mtDNA) is a small, typically circular molecule found in
²³⁶ most eukaryotes. It encodes essential genes involved in oxidative phosphorylation
²³⁷ and energy metabolism. Because of its conserved structure, mtDNA has become
²³⁸ a valuable genetic marker for studies in population genetics and phylogenetics
²³⁹ (Anderson et al., 1981; Boore, 1999). In animal species, the mitochondrial genome

240 ranges from 15–20 kilobase and contains 13 protein-coding genes, 22 tRNAs, and
241 two rRNAs arranged compactly without introns (Gray, 2012). In comparison to
242 nuclear DNA, the ratio of the number of copies of mtDNA is higher and has
243 simple organization which make it particularly suitable for genome sequencing
244 and assembly studies (Dierckxsens et al., 2017).

245 2.1.1 Mitochondrial Genome Assembly

246 Mitochondrial genome assembly refers to the reconstruction of the complete mito-
247 chondrial DNA (mtDNA) sequence from raw or fragmented sequencing reads. It is
248 conducted to obtain high-quality, continuous representations of the mitochondrial
249 genome that can be used for a wide range of analyses, including species identi-
250 fication, phylogenetic reconstruction, evolutionary studies, and investigations of
251 mitochondrial diseases. Because mtDNA evolves rapidly, its assembled sequence
252 provides valuable insights into population structure, lineage divergence, and adap-
253 tive evolution across taxa (Boore, 1999). Compared to nuclear genome assembly,
254 assembling the mitochondrial genome is often considered more straightforward but
255 still encounters technical challenges such as the formation of chimeric reads. Com-
256 monly used tools for mitogenome assembly such as GetOrganelle and MITObim
257 operate under the assumption of organelle genome circularity, and are vulnerable
258 when chimeric reads disrupt this circular structure, resulting in assembly errors
259 (Hahn et al., 2013; Jin et al., 2020).

260 2.2 PCR Amplification and Chimera Formation

261 PCR plays an important role in NGS library preparation, as it amplifies target
262 DNA fragments for downstream analysis. However as previously mentioned, the
263 amplification process can also introduce chimeric reads which compromises the
264 quality of the input reads supplied to sequencing or assembly workflows. Chimeras
265 typically arise when incomplete extension occurs during a PCR cycle. This causes
266 the DNA polymerase to switch from one template to another and generate hy-
267 brid recombinant molecules (Judo et al., 1998). Artificial chimeras are produced
268 through such amplification errors, whereas biological chimeras occur naturally
269 through genomic rearrangements or transcriptional events.

270 In the context of amplicon-based sequencing, the presence of chimeras can in-
271 flate estimates of genetic or microbial diversity and may cause misassemblies dur-
272 ing genome reconstruction. Qin et al. (2023) has reported that chimeric sequences
273 may account for more than 10% of raw reads in amplicon datasets. This artifact
274 tends to be most prominent among rare operational taxonomic units (OTUs) or
275 singletons, which are sometimes misinterpreted as novel diversity, further caus-
276 ing the complication of microbial diversity analyses (Gonzalez, Zimmermann, &
277 Saiz-Jimenez, 2004). As such, determining and minimizing PCR-induced chimera
278 formation is vital for improving the quality of mitochondrial genome assemblies,
279 and ensuring the reliability of amplicon sequencing data.

280 2.3 Existing Traditional Approaches for Chimera 281 Detection

Several computational tools have been developed to identify chimeric sequences in NGS datasets. These tools generally fall into two categories: reference-based and de novo approaches. Reference-based chimera detection, also known as database-dependent detection, is one of the earliest and most widely used computational strategies for identifying chimeric sequences in amplicon-based community studies. These methods rely on the comparison of each query sequence against a curated, high-quality database of known, non-chimeric reference sequences (Edgar et al., 2011).

290 On the other hand, the de novo chimera detection, also referred to as reference-
291 free detection, represents an alternative computational paradigm that identifies
292 chimeric sequences without reliance on external reference databases. This method
293 infer chimeras based on internal relationships among the sequences present within
294 the dataset itself, making it particularly advantageous in studies of under explored
295 or taxonomically diverse communities where comprehensive reference databases
296 are unavailable or incomplete (Edgar, 2016; Edgar et al., 2011). The underlying
297 assumption on this method is that during PCR, true biological sequences are
298 generally more abundant as they are amplified early and dominate the read pool,
299 whereas chimeric sequences appear later and are generally less abundant. The
300 de novo approach leverage this abundance hierarchy, treating the most abundant
301 sequences as supposed parents and testing whether less abundant sequences can
302 be reconstructed as mosaics of these templates. Compositional and structural
303 similarity are also evaluated to check whether different regions of a candidate

304 sequence correspond to distinct high-abundance sequences.

305 In practice, many modern bioinformatics pipelines combine both paradigms
306 sequentially: an initial de novo step identifies dataset-specific chimeras, followed
307 by a reference-based pass that removes remaining artifacts relative to established
308 databases (Edgar, 2016). These two methods of detection form the foundation of
309 tools such as UCHIME and later UCHIME2.

310 2.3.1 UCHIME

311 UCHIME is one of the most widely used tools for detecting chimeric sequences in
312 amplicon-based studies and remains a standard quality-control step in microbial
313 community analysis. Its core strategy is to test whether a query sequence (Q) can
314 be explained as a mosaic of two parent sequences, (A and B), and to score this
315 relationship using a structured alignment model (Edgar et al., 2011).

316 In reference mode, UCHIME divides the query into several segments and maps
317 them against a curated database of non-chimeric sequences. Candidate parents
318 are identified, and a three-way alignment is constructed. The algorithm assigns
319 “Yes” votes when different segments of the query match different parents and
320 “No” votes when the alignment contradicts a chimeric pattern. The final score
321 reflects the balance of these votes. In de novo mode, UCHIME operationalizes the
322 abundance-skew principle described earlier: high-abundance sequences are treated
323 as candidate parents, and lower-abundance sequences are evaluated as potential
324 mosaics. This makes the method especially useful when no reliable reference
325 database exists.

326 Although UCHIME is highly sensitive, it faces key constraints. Chimeras
327 formed from parents with very low divergence (below 0.8%) are difficult to detect
328 because they are nearly indistinguishable from sequencing errors. Accuracy in ref-
329 erence mode depends strongly on database completeness, while de novo detection
330 assumes that true parents are both present and sufficiently more abundant, such
331 conditions are not always met.

332 **2.3.2 UCHIME2**

333 UCHIME2 extends the original algorithm with refinements tailored for high-
334 resolution sequencing data. One of its major contributions is a re-evaluation
335 of benchmarking practices. Edgar (2016) demonstrated that earlier accuracy es-
336 timates for chimera detection were overly optimistic because they relied on un-
337 realistic scenarios where all true parent sequences were assumed to be present.
338 Using the more rigorous CHSIMA benchmark, UCHIME2 showed the prevalence
339 of “fake models” or real biological sequences that can be perfectly reconstructed
340 as apparent chimeras of other sequences, which suggests that perfect chimera de-
341 tection is theoretically unattainable. UCHIME2 also introduces several preset
342 modes (e.g., denoised, balanced, sensitive, specific, high-confidence) designed to
343 tune sensitivity and specificity depending on dataset characteristics. These modes
344 allow users to adjust the algorithm to the expected noise level or analytical goals.

345 Despite these improvements, UCHIME2 must be applied with caution. The
346 website manual explicitly advises against using UCHIME2 as a standalone
347 chimera-filtering step in OTU clustering or denoising workflows because doing so
348 can inflate both false positives and false negatives (Edgar, n.d.).

349 2.3.3 CATch

350 As previously mentioned, UCHIME (Edgar et al., 2011) relied on alignment-based
351 sequences in amplicon data. However, researchers soon observed that different al-
352 gorithms often produced inconsistent predictions. A sequence might be identified
353 as chimeric by one tool but classified as non-chimeric by another, resulting in
354 unreliable filtering outcomes across studies.

355 To address these inconsistencies, Mysara, Saeys, Leys, Raes, and Monsieurs
356 (2015) developed the Classifier for Amplicon Tool Chimeras (CATCh), which rep-
357 resents the first ensemble machine learning system designed for chimera detection
358 in 16S rRNA amplicon sequencing. Rather than depending on a single detec-
359 tion strategy, CATCh integrates the outputs of several established tools, includ-
360 ing UCHIME, ChimeraSlayer, DECIPHER, Pintail, and Perseus. The individual
361 scores and binary decisions generated by these tools are used as input features for
362 a supervised learning model. The algorithm employs a Support Vector Machine
363 (SVM) with a Pearson VII Universal Kernel (PUK) to determine optimal weight-
364 ings among the input features and to assign each sequence a probability of being
365 chimeric.

366 Benchmarking in both reference-based and de novo modes demonstrated signif-
367 icant performance improvements. CATCh achieved sensitivities of approximately
368 85 percent in reference-based mode and 92 percent in de novo mode, with corre-
369 sponding specificities of approximately 96 percent and 95 percent. These results
370 indicate that CATCh detected 7 to 12 percent more chimeras than any individual
371 algorithm while maintaining high precision.

372 2.3.4 ChimPipe

373 Among the available tools for chimera detection, ChimPipe is a pipeline developed
374 to identify chimeric sequences such as biological chimeras. It uses both discordant
375 paired-end reads and split-read alignments to improve the accuracy and sensitivity
376 of detecting biological chimeras (Rodriguez-Martin et al., 2017). By combining
377 these two sources of information, ChimPipe achieves better precision than meth-
378 ods that depend on a single type of indicator.

379 The pipeline works with many eukaryotic species that have available genome
380 and annotation data (Rodriguez-Martin et al., 2017). It can also predict multiple
381 isoforms for each gene pair and identify breakpoint coordinates that are useful
382 for reconstructing and verifying chimeric transcripts. Tests using both simulated
383 and real datasets have shown that ChimPipe maintains high accuracy and reliable
384 performance.

385 ChimPipe lets users adjust parameters to fit different sequencing protocols or
386 organism characteristics. Experimental results have confirmed that many chimeric
387 transcripts detected by the tool correspond to functional fusion proteins, demon-
388 strating its utility for understanding chimera biology and its potential applications
389 in disease research (Rodriguez-Martin et al., 2017).

390 **2.4 Machine Learning Approaches for Chimera**

391 **and Sequence Quality Detection**

392 Traditional chimera detection tools rely primarily on heuristic or alignment-based
393 rules. Recent advances in machine learning (ML) have demonstrated that models
394 trained on sequence-derived features can effectively capture compositional and
395 structural patterns in biological sequences. Although most existing ML systems
396 such as those used for antibiotic resistance prediction, taxonomic classification,
397 or viral identification are not specifically designed for chimera detection, they
398 highlight how data-driven models can outperform similarity-based heuristics by
399 learning intrinsic sequence signatures. In principle, ML frameworks can integrate
400 indicators such as k-mer frequencies, GC-content variation and split-alignment
401 metrics to identify subtle anomalies that may indicate a chimeric origin (Arango
402 et al., 2018; Liang, Bible, Liu, Zou, & Wei, 2020; Ren et al., 2020).

403 **2.4.1 Feature-Based Representations of Genomic Se-**

404 **quences**

405 Feature extraction converts DNA sequences into numerical representations suit-
406 able for machine learning models. One approach is k-mer frequency analysis,
407 which counts short nucleotide sequences within a read (Vervier, Mahé, Tournoud,
408 Veyrieras, & Vert, 2015). High-frequency k-mers, including simple repeats such
409 as “AAAAAA,” can highlight repetitive or unusual regions that may occur near
410 chimeric junctions. Comparing k-mer patterns across adjacent parts of a read can
411 help identify such regions, while GC content provides an additional descriptor of

412 local sequence composition (Ren et al., 2020).

413 Alignment-derived features further inform junction detection. Long-read tools
414 such as Sniffles (Sedlazeck et al., 2018) use split alignments to locate breakpoints
415 across extended sequences, whereas short-read aligners like Minimap2 (Li, 2018)
416 report supplementary and secondary alignments that indicate local discontinu-
417 ities. Split alignments, where parts of a read map to different regions, can reveal
418 template-switching events. These features complement k-mer profiles and en-
419 hance detection of potentially chimeric reads, even in datasets with incomplete
420 references.

421 Microhomology, or short sequences shared between adjacent segments, is an-
422 other biologically meaningful feature. Short microhomologies, typically 3–20 bp,
423 are involved in template switching both in cellular repair pathways and during
424 PCR, where they act as signatures of chimera formation (Peccoud et al., 2018;
425 Sfeir & Symington, 2015). In PCR-induced chimeras, short identical sequences
426 at junctions provide a clear signature of chimerism. Measuring the longest exact
427 overlap at each breakpoint complements k-mer and alignment features and helps
428 identify reads that are potentially chimeric.

429 **2.5 Synthesis of Chimera Detection Approaches**

430 To provide an integrated overview of the literature discussed in this chapter, Ta-
431 ble 2.1 summarizes the major chimera detection studies, their methodological
432 approaches, and their known limitations.

Table 2.1: Comparison of Chimera Detection Approaches and Tools

Method / Tool	Core Approach	Key Limitations
Reference-based Detection	Compares each query sequence against curated databases of verified, non-chimeric sequences; evaluates segment similarity to identify mosaic patterns.	Accuracy depends on database completeness; performs poorly for novel taxa or missing parents; limited sensitivity for low-divergence chimeras.
De novo Detection	Identifies chimeras using only internal dataset structure; leverages abundance hierarchy and compositional similarity to infer whether low-abundance sequences can be reconstructed from abundant parents.	Assumes true sequences are more abundant; fails when amplification bias distorts abundances; struggles when parental sequences are similarly abundant or highly similar.
UCHIME	Alignment-based model that partitions the query into segments, identifies parent candidates, and computes a chimera score via a three-way alignment; supports reference and de novo modes.	Reduced accuracy for very closely related parents (<0.8% divergence); sensitive to incomplete databases; de novo mode fails if parents are absent or not sufficiently more abundant.
UCHIME2	Updated UCHIME with improved benchmarking (CHSIMA) and multiple sensitivity/specificity presets; better handles incomplete references and dataset variability.	“Fake models” limit theoretical accuracy; genuine variants may mimic chimeras; not recommended as a standalone step in OTU or denoising pipelines due to increased false positives/negatives.
CATCh	First ensemble ML model for 16S chimera detection; integrates outputs of UCHIME, ChimeraSlayer, DECIPHER, Pintail, and Perseus using an SVM to boost overall prediction accuracy.	Performance constrained by underlying tools; ML model cannot capture features not present in component algorithms; may misclassify in highly novel or low-coverage datasets.
ChimPipe	Pipeline for detecting biological chimeras in RNA-seq using discordant paired-end reads and split-read alignments; identifies isoforms and breakpoint coordinates.	Requires high-quality genome and annotation; tailored to RNA-seq rather than amplicons; computationally intensive; limited to organisms with available reference genomes.

433 Across existing studies, no single approach reliably detects all forms of chimeric
434 sequences, and the reviewed literature consistently shows that chimeras remain a
435 persistent challenge in genomics and bioinformatics. Although the surveyed tools
436 are not designed specifically for organelle genome assembly, they provide valua-
437 ble insights into which methodological strategies are effective and where current
438 approaches fall short. These limitations collectively define a clear research gap:
439 the need for a specialized, feature-driven detection framework tailored to PCR-
440 induced mitochondrial chimeras. Addressing this gap aligns with the research
441 objective outlined in Section 1.3, which is to develop and evaluate a machine
442 learning-based pipeline (MitoChime) that improves the quality of downstream
443 mitochondrial genome assembly. In support of this aim, the subsequent chapters
444 describe the design, implementation, and evaluation of the proposed tool.

⁴⁴⁵ Chapter 3

⁴⁴⁶ Research Methodology

⁴⁴⁷ This chapter outlines the steps involved in completing the study, including data
⁴⁴⁸ gathering, generating simulated mitochondrial Illumina reads, preprocessing and
⁴⁴⁹ indexing the data, developing a feature extraction pipeline to obtain read-level fea-
⁴⁵⁰ tures, applying machine learning algorithms for chimera detection, implementing
⁴⁵¹ feature selection methods, and validating and comparing model performance.

⁴⁵² 3.1 Research Activities

⁴⁵³ As illustrated in Figure 3.1, this study carried out a sequence of procedures to
⁴⁵⁴ detect PCR-induced chimeric reads in mitochondrial genomes. The process began
⁴⁵⁵ with collecting a mitochondrial reference sequence of *Sardinella lemuru* from the
⁴⁵⁶ National Center for Biotechnology Information (NCBI) database, which was used
⁴⁵⁷ as a reference for generating simulated clean and chimeric reads. These reads
⁴⁵⁸ were subsequently indexed and mapped. The resulting collections then passed

459 through a feature extraction pipeline that computed k-mer profiles, supplementary
460 alignment (SA) features, and microhomology information to prepare the data
461 for model construction. The machine learning models were trained using the
462 processed input, evaluated using cross-validation and held-out testing, tuned for
463 improved performance, and then subjected to feature importance and feature
464 selection analyses before final validation.

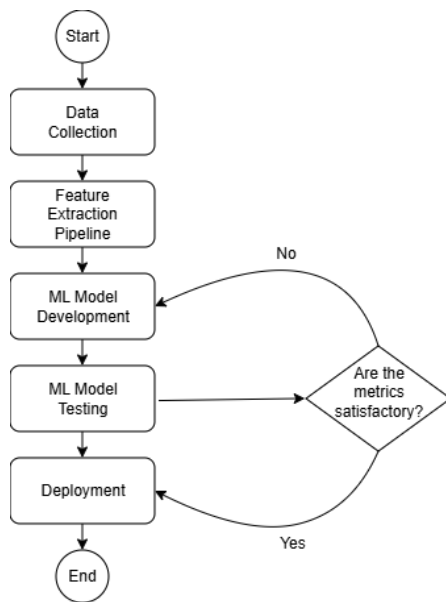


Figure 3.1: Process diagram of the study workflow.

465 3.1.1 Data Collection

466 The mitochondrial genome reference sequence of *S. lemuru* was obtained from the
467 NCBI database (accession number NC_039553.1) in FASTA format and was used
468 to generate simulated reads.

469 This step was scheduled to begin in the first week of November 2025 and
470 expected to be completed by the end of that week, with a total duration of ap-

471 proximately one (1) week.

472 Data Preprocessing

473 All steps in the simulation and preprocessing pipeline were executed using a cus-
474 tom script in Python (Version 3.11). The script runs each stage, including read
475 simulation, reference indexing, mapping, and alignment processing, in a fixed se-
476 quence.

477 `wgsim` (Version 1.13) was used to simulate 10,000 paired-end fragments, pro-
478 ducing 20,000 reads (10,000 forward and 10,000 reverse) from the original refer-
479 ence (`original_reference.fasta`) and designated as clean reads. The tool was
480 selected because it provides fast generation of Illumina-like reads with controllable
481 error rates, using the following command:

```
482 wgsim -1 150 -2 150 -r 0 -R 0 -X 0 -e 0.05 -N 10000 \
483           original_reference.fasta ref1.fastq ref2.fastq
```

484 Chimeric sequences were then generated from the same reference FASTA
485 file using a separate Python script. Two non-adjacent segments were ran-
486 domly selected such that their midpoint distances fell within specified minimum
487 and maximum thresholds. The script attempted to retain microhomology to
488 mimic PCR-induced template switching. The resulting chimeras were written
489 to `chimera_reference.fasta` and processed with `wgsim` to simulate 10,000
490 paired-end fragments, generating 20,000 chimeric reads (10,000 forward reads in
491 `chimeric1.fastq` and 10,000 reverse reads in `chimeric2.fastq`) using the same
492 command format as above.

493 Next, a `minimap2` index of the reference genome was created using:

```
494  minimap2 -d ref.mmi original_reference.fasta
```

495 Minimap2 (Version 2.28) was used to map simulated clean and chimeric reads
496 to the original reference. An index (`ref.mmi`) was first generated to enable efficient
497 alignment, and mapping produced the alignment features used as input for the
498 machine learning model. The reads were mapped using the following commands:

```
499  minimap2 -ax sr -t 8 ref.mmi ref1.fastq ref2.fastq > clean.sam
```

```
500  minimap2 -ax sr -t 8 ref.mmi \  
501        chimeric1.fastq chimeric2.fastq > chimeric.sam
```

502 The resulting clean and chimeric SAM files contain the alignment positions of
503 each read relative to the original reference genome. These files were then converted
504 to BAM format, sorted, and indexed using `samtools` (Version 1.20):

```
505  samtools view -bS clean.sam -o clean.bam  
506  samtools view -bS chimeric.sam -o chimeric.bam  
507  
508  samtools sort clean.bam -o clean.sorted.bam  
509  samtools index clean.sorted.bam  
510  
511  samtools sort chimeric.bam -o chimeric.sorted.bam  
512  samtools index chimeric.sorted.bam
```

513 The total number of simulated reads was expected to be 40,000. The final col-
514 lection of reads contained 19,984 clean reads and 20,000 chimeric reads (39,984 en-
515 tries in total), providing a roughly balanced distribution between the two classes.
516 After alignment with `minimap2`, only 19,984 clean reads remained because un-
517 mapped reads were not included in the BAM file. Some sequences failed to align
518 due to the error rate defined during `wgsim` simulation, which produced mismatches
519 that caused certain reads to fall below the aligner’s matching threshold.

520 This whole process was scheduled to start in the second week of November 2025
521 and was expected to be completed by the last week of November 2025, with a total
522 duration of approximately three (3) weeks.

523 **3.1.2 Feature Extraction Pipeline**

524 This stage directly followed the alignment phase, utilizing the resulting BAM files
525 (specifically `chimeric.sorted.bam` and `clean.sorted.bam`). A custom Python
526 script was created to efficiently process each primary-mapped read to extract
527 the necessary set of features, which were then compiled into a structured feature
528 matrix in TSV format. The pipeline’s core functionality relied on the `Pysam`
529 (Version 0.22) library for parsing BAM structures and `NumPy` (Version 1.26) for
530 array operations and computations. To ensure correctness and adherence to best
531 practices, bioinformatics experts at PGC Visayas were consulted to validate the
532 pipeline design, feature extraction logic, and overall data integrity.

533 This stage of the study was scheduled to begin in the last week of Novem-
534 ber 2025 and conclude by the first week of December 2025, with an estimated

535 total duration of approximately two (2) weeks.

536 The pipeline focused on three feature families that collectively capture bi-
537 ological signatures associated with PCR-induced chimeras: (1) supplementary
538 alignment (SA) and alignment-structure metrics, (2) k-mer composition differ-
539 ence, and (3) microhomology around putative junctions. Additional alignment
540 quality indicators such as mapping quality were also included.

541 **Supplementary Alignment and Alignment-Structure Features**

542 Split-alignment information was derived from the SA tag embedded in each pri-
543 mary read of the BAM file. This tag is typically associated with reads that map to
544 multiple genomic locations, suggesting a chimeric structure. To extract this infor-
545 mation, the script first checked whether the read carried an **SA:Z** tag. If present,
546 the tag string was parsed using the function **parse_sa_tag**, yielding metadata for
547 each alignment containing the reference name, mapped position, strand, mapping
548 quality, and number of mismatches.

549 After parsing, the function **sa_feature_stats** was applied to establish the fun-
550 damental split indicators, **has_sa** and **sa_count**. Along with these initial counts,
551 the function aggregated metrics related to the structure and reliability of the
552 split alignments, including the number of alignment segments, strand consistency,
553 minimum, maximum, and mean distance between split segments, and summary
554 statistics of mapping quality and mismatch counts across segments.

555 **K-mer Composition Difference**

556 Comparing k-mer frequency profiles between the left and right halves of a read
557 allows for the detection of abrupt compositional shifts, independent of alignment
558 information.

559 The script implemented this by inferring a likely junction breakpoint using the
560 function `infer_breakpoints`, prioritizing the boundaries defined by soft-clipping
561 operations. If no clipping was present, the midpoint of the alignment or the read
562 length was used as a fallback. The read sequence was then divided into left and
563 right segments at this inferred breakpoint, and k-mer frequency profiles ($k =$
564 6) were generated for both halves, ignoring any k-mers containing ambiguous N
565 bases. The resulting k-mer frequency vectors were normalised and compared using
566 the functions `cosine_difference` and `js_divergence` to quantify compositional
567 discontinuity across the inferred breakpoint.

568 **Microhomology**

569 The process of extracting the microhomology feature also started by using
570 `infer_breakpoints` to identify a candidate junction. Once a breakpoint was
571 established, the script scanned a ± 40 base-pair window surrounding the break-
572 point and applied the function `longest_suffix_prefix_overlap` to identify the
573 longest exact suffix-prefix overlap between the left and right read segments. This
574 overlap, representing consecutive bases shared at the junction, was recorded as
575 `microhomology_length` in the dataset. The 40 base-pair window was chosen
576 to ensure that short shared sequences at or near the breakpoint were captured

577 without including distant sequences that are unlikely to be mechanistically
578 related.

579 Additionally, the GC content of the overlapping sequence was calculated using
580 the function `gc_content`, which counts guanine (G) and cytosine (C) bases within
581 the detected microhomology and divides by the total length, yielding a proportion
582 between 0 and 1 that was stored under the `microhomology_gc` attribute. Micro-
583 homology was quantified using a 3–20 bp window, consistent with values reported
584 in prior research on PCR-induced chimeras. A k-mer length of 6 was used to cap-
585 ture patterns within the 40 bp window surrounding each breakpoint, providing
586 sufficient resolution to detect informative sequence shifts.

587 3.1.3 Machine Learning Model Development

588 After feature extraction, the per-read feature matrices for clean and chimeric
589 reads were merged into a single dataset. Each row corresponded to one paired-
590 end read, and columns encoded alignment-structure features (e.g., supplementary
591 alignment count and spacing between segments), CIGAR-derived soft-clipping
592 statistics (e.g., left and right soft-clipped length, total clipped bases), k-mer com-
593 position discontinuity between read segments, microhomology descriptors near
594 candidate junctions, and alignment quality (e.g., mapping quality). The result-
595 ing feature set comprised 23 numeric features and was restricted to quantities
596 that can be computed from standard BAM/FASTQ files in typical mitochondrial
597 sequencing workflows.

598 The labelled dataset was randomly partitioned into training (80%) and test

599 (20%) subsets using stratified sampling to preserve the 1:1 ratio of clean to
600 chimeric reads. Model development and evaluation were implemented in Python
601 (Version 3.11) using the `scikit-learn`, `xgboost`, `lightgbm`, and `catboost` li-
602 braries. A broad panel of classification algorithms was then benchmarked on the
603 training data to obtain a fair comparison of different model families under identical
604 feature conditions. The panel included a trivial dummy classifier, L_2 -regularized
605 logistic regression, a calibrated linear support vector machine (SVM), k -nearest
606 neighbours, Gaussian Naïve Bayes, decision-tree ensembles (Random Forest, Ex-
607 tremely Randomized Trees, and Bagging with decision trees), gradient boosting
608 methods (Gradient Boosting, XGBoost, LightGBM, and CatBoost), and a shallow
609 multilayer perceptron (MLP).

610 For each model, five-fold stratified cross-validation was performed on the train-
611 ing set. In every fold, four-fifths of the data were used for fitting and the remaining
612 one-fifth for validation. Mean cross-validation accuracy, precision, recall, F1-score
613 for the chimeric class, and area under the receiver operating characteristic curve
614 (ROC–AUC) were computed to summarize performance and rank candidate meth-
615 ods. This baseline screen allowed comparison of linear, probabilistic, neural, and
616 ensemble-based approaches and identified tree-based ensemble and boosting mod-
617 els as consistently strong performers relative to simpler baselines.

618 **3.1.4 Model Benchmarking, Hyperparameter Optimiza- 619 tion, and Evaluation**

620 Model selection and refinement proceeded in two stages. First, the cross-validation
621 results from the broad panel were used to identify a subset of competitive mod-

els for more detailed optimization. Specifically, ten model families were carried forward: L_2 -regularized logistic regression, calibrated linear SVM, Random Forest, ExtraTrees, Gradient Boosting, XGBoost, LightGBM, CatBoost, Bagging with decision trees, and a shallow MLP. This subset spans both linear and non-linear decision boundaries, but emphasizes ensemble and boosting methods, which showed superior F1 and ROC–AUC in the initial benchmark.

Second, hyperparameter optimization was conducted for each of the ten selected models using randomized search with five-fold stratified cross-validation (`RandomizedSearchCV`). For tree-based ensembles, the search space included the number of trees, maximum depth, minimum samples per split and per leaf, and the fraction of features considered at each split. For boosting methods, key hyperparameters such as the number of boosting iterations, learning rate, tree depth, subsampling rate, and column subsampling rate were tuned. For the MLP, the number and size of hidden layers, learning rate, and L_2 -regularization strength were varied. In all cases, the primary optimisation criterion was the F1-score of the chimeric class, averaged across folds.

For each model family, the hyperparameter configuration with the highest mean cross-validation F1-score was selected as the best-tuned estimator. These tuned models were then refitted on the full training set and evaluated once on the held-out test set to obtain unbiased estimates of performance. Test-set metrics included accuracy, precision, recall, F1-score for the chimeric class, and ROC–AUC. Confusion matrices and ROC curves were generated for the top-performing models to characterise common error modes, such as false negatives (missed chimeric reads) and false positives (clean reads incorrectly labelled as chimeric). The final model or small set of models for downstream interpretation was chosen based on

647 a combination of test-set F1-score and ROC–AUC.

648 3.1.5 Feature Importance, Feature Selection, and Interpretation

650 To relate model decisions to biologically meaningful signals, feature-importance
651 analyses were performed on the best-performing tree-based models. Two comple-
652 mentary approaches were used. First, built-in importance measures from ensemble
653 methods (e.g., split-based importances in Random Forest and Gradient Boosting)
654 were examined to obtain an initial ranking of features based on their contributition
655 to reducing impurity. Second, model-agnostic permutation importance was com-
656 puted on the test set by repeatedly permuting each feature column while keeping
657 all others fixed and measuring the resulting decrease in F1-score. Features whose
658 permutation led to a larger performance drop were interpreted as more influential
659 for chimera detection.

660 For interpretability, individual features were grouped into conceptual families:
661 (i) supplementary alignment and alignment-structure features (e.g., SA count,
662 spacing between alignment segments, strand consistency), (ii) soft-clipping fea-
663 tures (e.g., left and right soft-clipped length, total clipped bases, inferred break-
664 point position), (iii) k-mer composition discontinuity features (e.g., cosine dis-
665 tance and Jensen–Shannon divergence between k-mer profiles of read segments),
666 (iv) microhomology descriptors (e.g., microhomology length and local GC content
667 around putative breakpoints), and (v) other alignment quality features (e.g., map-
668 ping quality). This analysis provided a basis for interpreting the trained models
669 in terms of known mechanisms of PCR-induced template switching and for iden-

670 tifying which alignment-based and sequence-derived cues are most informative for
671 distinguishing chimeric from clean mitochondrial reads.

672 Building on these importance results, an explicit feature selection step was
673 implemented using CatBoost as the reference model, since it was among the top-
674 performing classifiers. Permutation importance scores were re-estimated for Cat-
675 Boost on the held-out test set using the F1-score of the chimeric class as the
676 scoring function. Negative importance scores, which indicate that permuting a
677 feature did not reliably harm performance, were set to zero and interpreted as
678 noise. The remaining non-negative importances were sorted in descending order
679 and converted into a cumulative importance curve by expressing each feature's
680 importance as a fraction of the total positive importance.

681 A compact feature subset was then defined by selecting the smallest number of
682 features whose cumulative importance reached at least 95% of the total positive
683 importance. This procedure yielded a reduced set of four strongly predictive
684 variables dominated by soft-clipping and k-mer divergence metrics (for example,
685 total clipped bases and k-mer divergence between read halves).

686 To quantify the impact of this reduction, CatBoost was retrained using only
687 the selected feature subset, with the same tuned hyperparameters as the full 23-
688 feature model, and evaluated on the held-out test set. Performance of the reduced
689 model was then compared to that of the full model in terms of F1-score and ROC–
690 AUC to assess whether dimensionality could be reduced without appreciable loss
691 in predictive accuracy.

692 In addition, an ablation experiment was performed to specifically evaluate
693 the contribution of explicit microhomology features. The microhomology vari-

ables (`microhomology_length` and `microhomology_gc`) were removed from the full feature set to obtain a 21-feature configuration. CatBoost was refitted on this microhomology-ablated feature set, using the same tuned hyperparameters, and evaluated on the held-out test set. Comparing the full, reduced-subset, and microhomology-ablated variants allowed the study to quantify both the degree of redundancy among features and the practical contribution of microhomology to classification accuracy.

Taken together, the feature importance and feature selection analyses provided a more parsimonious model variant and a clearer interpretation of which alignment-based and sequence-derived signals are most informative for detecting PCR-induced chimeras.

3.1.6 Validation and Testing

Validation involved both internal and external evaluations. Internal validation was achieved through five-fold stratified cross-validation on the training data to verify model generalization and reduce variance due to random sampling. External testing was performed on the 20% hold-out dataset from the simulated reads, providing an unbiased assessment of model generalization. Feature extraction and preprocessing were applied consistently across all splits.

Comparative evaluation was performed across all candidate algorithms and CatBoost feature-set variants to determine which models demonstrated the highest predictive performance and computational efficiency under identical data conditions. Their metrics were compared to identify which algorithms and feature

716 configurations were most suitable for further refinement and potential integration
717 into downstream mitochondrial assembly workflows.

718 3.1.7 Documentation

719 Comprehensive documentation was maintained throughout the study to ensure
720 transparency and reproducibility. All stages of the research, including data gath-
721 ering, preprocessing, feature extraction, model training, feature selection, and
722 validation, were systematically recorded in a `README` file in the GitHub reposi-
723 tory. For each analytical step, the corresponding parameters, software versions,
724 and command line scripts were documented to enable exact replication of results.

725 The repository structure followed standard research data management prac-
726 tices, with clear directories for datasets and scripts. Computational environments
727 were standardised using Conda, with an environment file (`environment.yml`)
728 specifying dependencies and package versions to maintain consistency across sys-
729 tems.

730 For manuscript preparation and supplementary materials, Overleaf (\LaTeX)
731 was used to produce publication-quality formatting and consistent referencing.

732 3.2 Calendar of Activities

733 Table 3.1 presents the project timeline in the form of a Gantt chart, where each
734 bullet point corresponds to approximately one week of planned activity.

Table 3.1: Timetable of activities.

Activities (2025)	Nov	Dec	Jan	Feb	Mar	Apr	May
Data Collection and Simulation	• • • •						
Feature Extraction Pipeline	•	•					
Machine Learning Development		•	• •	• • • •	• • • •	• •	
Testing and Validation						• •	• • • •
Documentation	• • • •	• • • •	• • • •	• • • •	• • • •	• • • •	• • • •

⁷³⁵ Chapter 4

⁷³⁶ Results and Discussion

⁷³⁷ 4.1 Descriptive Analysis of Features

⁷³⁸ This chapter presents the performance of the proposed feature set and machine
⁷³⁹ learning models for detecting PCR-induced chimeric reads in simulated mitochon-
⁷⁴⁰ drial Illumina data. The behaviour of the main features is first described, followed
⁷⁴¹ by a comparison of baseline classifiers, an assessment of the effect of hyperparam-
⁷⁴² eter tuning, and an analysis of feature importance in terms of individual variables
⁷⁴³ and feature families.

⁷⁴⁴ The final dataset contained 31,986 reads for training and 7,997 reads for test-
⁷⁴⁵ ing, with classes balanced (approximately 4,000 clean and 4,000 chimeric reads in
⁷⁴⁶ the test split).

747 4.1.1 Exploratory Data Analysis

748 An exploratory data analysis (EDA) was conducted on the extracted feature ma-
749 trix to characterize general patterns in the data and gain preliminary insight into
750 which variables might meaningfully contribute to classification. Histograms of key
751 features indicated that alignment-based variables showed clear class separation as
752 chimeric reads have higher frequencies of split alignments and broader long-tailed
753 distribution on soft-clipped regions (`softclip_left` and `softclip_right`). In
754 contrast, sequence-based variables such a microhomology length and k-mer di-
755 vergence displayed substantial overlap between classes, suggesting more limited
756 discriminative value. The complete set of histograms is provided in Appendix A.

757 As shown in Figure 4.1, the feature correlation heatmap shows that alignment-
758 derived features form a strongly correlated cluster, whereas sequence-derived fea-
759 tures show weak correlations with both the alignment-based features and with
760 one another. This heterogeneity indicates that no single feature family captures
761 all relevant signal sources.

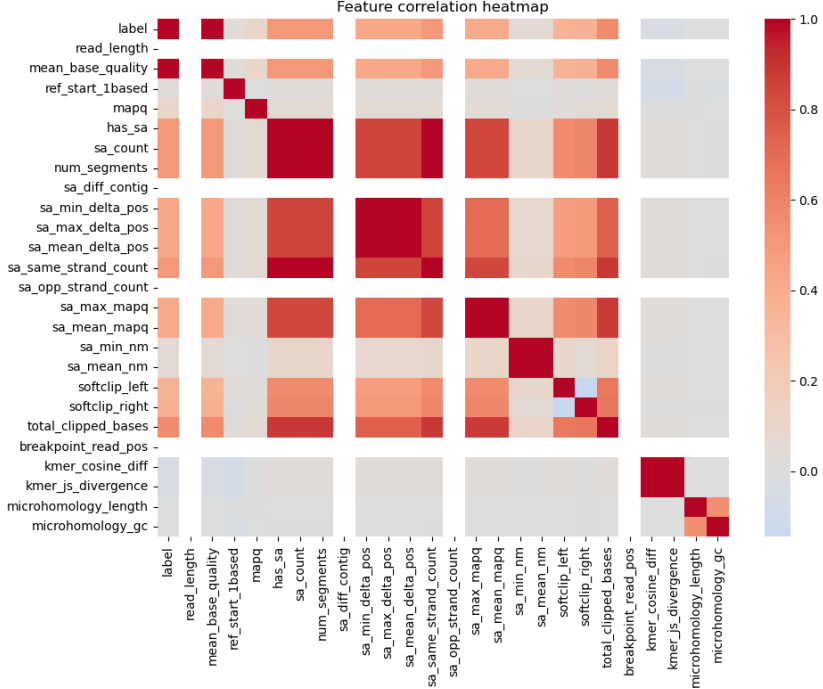


Figure 4.1: Feature correlation heatmap showing relationships among alignment-derived and sequence-derived features.

762 4.2 Baseline Classification Performance

763 Table 4.1 summarises the performance of eleven classifiers trained on the engi-
 764 neered feature set using five-fold cross-validation and evaluated on the held-out
 765 test set. All models were optimised using default hyperparameters, without ded-
 766 icated tuning.

767 The dummy baseline, which always predicts the same class regardless of the
 768 input features, achieved an accuracy of 0.50 and test F1-score of 0.67. This re-
 769 flects the balanced class distribution and provides a lower bound for meaningful
 770 performance.

771 Across other models, test F1-scores clustered in a narrow band between ap-
 772 proximately 0.74 and 0.77 and ROC–AUC values between 0.82 and 0.84. Gradi-
 773 ent boosting, CatBoost, LightGBM, XGBoost, bagging trees, random forest, and
 774 multilayer perceptron (MLP) all produced very similar scores, with CatBoost and
 775 gradient boosting slightly ahead (test F1 \approx 0.77, ROC–AUC \approx 0.84). Linear
 776 models (logistic regression and calibrated linear SVM) performed only marginally
 777 worse (test F1 \approx 0.74), while Gaussian Naive Bayes lagged behind with substan-
 778 tially lower F1 (\approx 0.65) despite very high precision for the chimeric class.

Table 4.1: Performance of baseline classifiers on the held-out test set.

model	test_accuracy	test_precision	test_recall	test_f1	test_roc_auc
dummy_baseline	0.500000	0.500000	1.000000	0.667000	0.500000
logreg_l2	0.789000	0.945000	0.614000	0.744000	0.821000
linear_svm_calibrated	0.789000	0.945000	0.614000	0.744000	0.820000
random_forest	0.788000	0.894000	0.654000	0.755000	0.834000
extra_trees	0.788000	0.901000	0.647000	0.753000	0.824000
gradient_boosting	0.802000	0.936000	0.648000	0.766000	0.840000
xgboost	0.800000	0.929000	0.650000	0.765000	0.839000
lightgbm	0.799000	0.926000	0.650000	0.764000	0.838000
catboost	0.803000	0.936000	0.650000	0.767000	0.839000
knn	0.782000	0.892000	0.642000	0.747000	0.815000
gaussian_nb	0.741000	0.996000	0.483000	0.651000	0.819000
bagging_trees	0.792000	0.900000	0.657000	0.760000	0.837000
mlp	0.789000	0.931000	0.625000	0.748000	0.819000

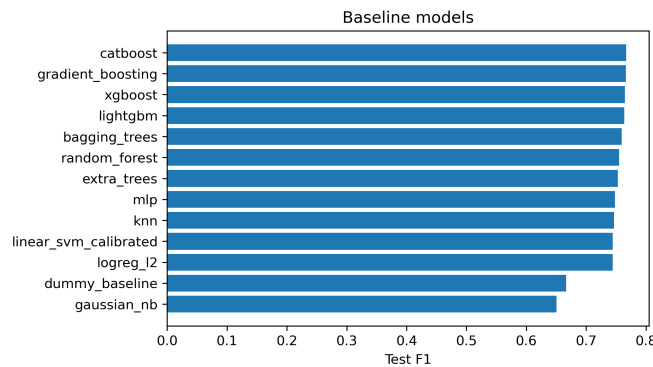


Figure 4.2: Test F1 of all baseline classifiers, showing that no single model clearly dominates and several achieve comparable performance.

779 4.3 Effect of Hyperparameter Tuning

780 To assess whether performance could be improved further, ten model families un-
781 derwent randomised hyperparameter search. The tuned metrics are summarised
782 in Table 4.2. Overall, tuning yielded modest but consistent gains for tree-based en-
783 sembles and boosting methods, while leaving linear models essentially unchanged
784 or slightly worse.

785 CatBoost, gradient boosting, LightGBM, XGBoost, random forest, bagging
786 trees, and MLP all experienced small increases in test F1 (typically $\Delta F1 \approx 0.002$ –
787 0.009) and ROC–AUC (up to $\Delta AUC \approx 0.008$). After tuning, CatBoost remained
788 the best performer with test accuracy 0.80, precision 0.92, recall 0.66, F1-score
789 0.77, and ROC–AUC 0.84. Gradient boosting achieved almost identical perfor-
790 mance (F1 0.77, AUC 0.84). Random forest and bagging trees also improved to
791 F1 scores around 0.76 with AUC ≈ 0.84 .

Table 4.2: Performance of tuned classifiers on the held-out test set.

model	test_accuracy	test_precision	test_recall	test_f1	test_roc_auc
logreg_l2_tuned	0.788000	0.946000	0.612000	0.743000	0.818000
linear_svm_calibrated_tuned	0.788000	0.944000	0.612000	0.743000	0.818000
random_forest_tuned	0.797000	0.915000	0.655000	0.763000	0.842000
extra_trees_tuned	0.794000	0.910000	0.652000	0.760000	0.837000
gradient_boosting_tuned	0.802000	0.928000	0.654000	0.767000	0.843000
xgboost_tuned	0.799000	0.922000	0.653000	0.765000	0.839000
lightgbm_tuned	0.801000	0.930000	0.651000	0.766000	0.842000
catboost_tuned	0.802000	0.924000	0.658000	0.769000	0.844000
bagging_trees_tuned	0.798000	0.922000	0.650000	0.763000	0.842000
mlp_tuned	0.790000	0.934000	0.625000	0.749000	0.821000

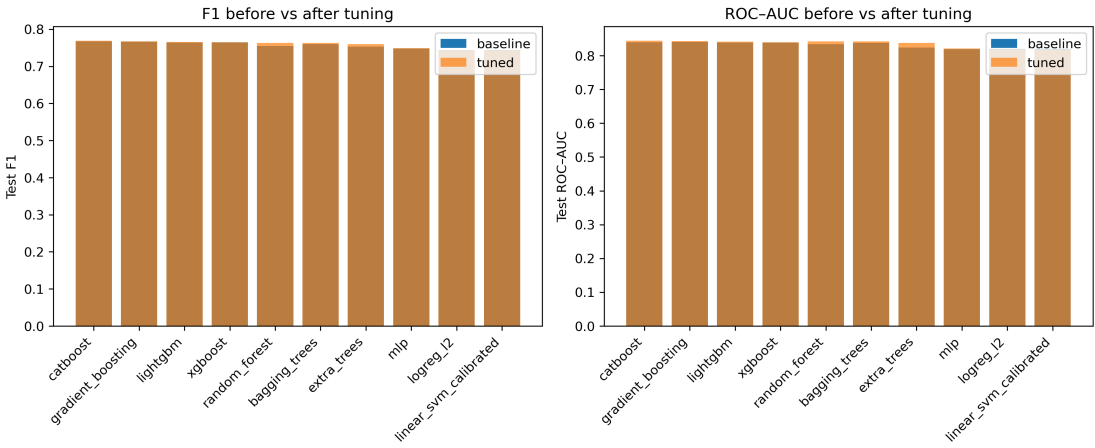


Figure 4.3: Comparison of test F1 (left) and ROC–AUC (right) for baseline and tuned models.

792 Because improvements are small and within cross-validation variability, tun-
 793 ing was interpreted as stabilising and slightly refining the models rather than
 794 completely altering their behaviour or their relative ranking.

795 4.4 Detailed Evaluation of Representative Mod- 796 els

797 For interpretability and diversity, four tuned models were selected for deeper
 798 analysis: CatBoost (best-performing boosted tree), scikit-learn gradient boost-
 799 ing (canonical gradient-boosting implementation), random forest (non-boosted
 800 ensemble baseline), and L_2 -regularised logistic regression (linear baseline). All
 801 models were trained on the engineered feature set and evaluated on the same
 802 held-out test data.

803 4.4.1 Confusion Matrices and Error Patterns

804 Classification reports and confusion matrices for the four models reveal consistent
805 patterns. CatBoost and gradient boosting both reached overall accuracy of ap-
806 proximately 0.80 with similar macro-averaged F1 scores (~ 0.80). For CatBoost,
807 precision and recall for clean reads were 0.73 and 0.95, respectively, while for
808 chimeric reads they were 0.92 and 0.66 ($F1 = 0.77$). Gradient boosting showed
809 nearly identical trade-offs.

810 Random forest attained slightly lower accuracy (0.80) and chimeric F1 (0.76),
811 whereas logistic regression achieved the lowest accuracy among the four (0.79)
812 and chimeric F1 (0.74), although it provided the highest chimeric precision (0.95)
813 at the cost of lower recall (0.61).

814 Across all models, errors were asymmetric. False negatives (chimeric reads
815 predicted as clean) were more frequent than false positives. For example, CatBoost
816 misclassified 1,369 chimeric reads as clean but only 215 clean reads as chimeric.
817 This pattern indicates that the models are conservative and prioritise avoiding
818 false chimera calls at the expense of missing some true chimeras.

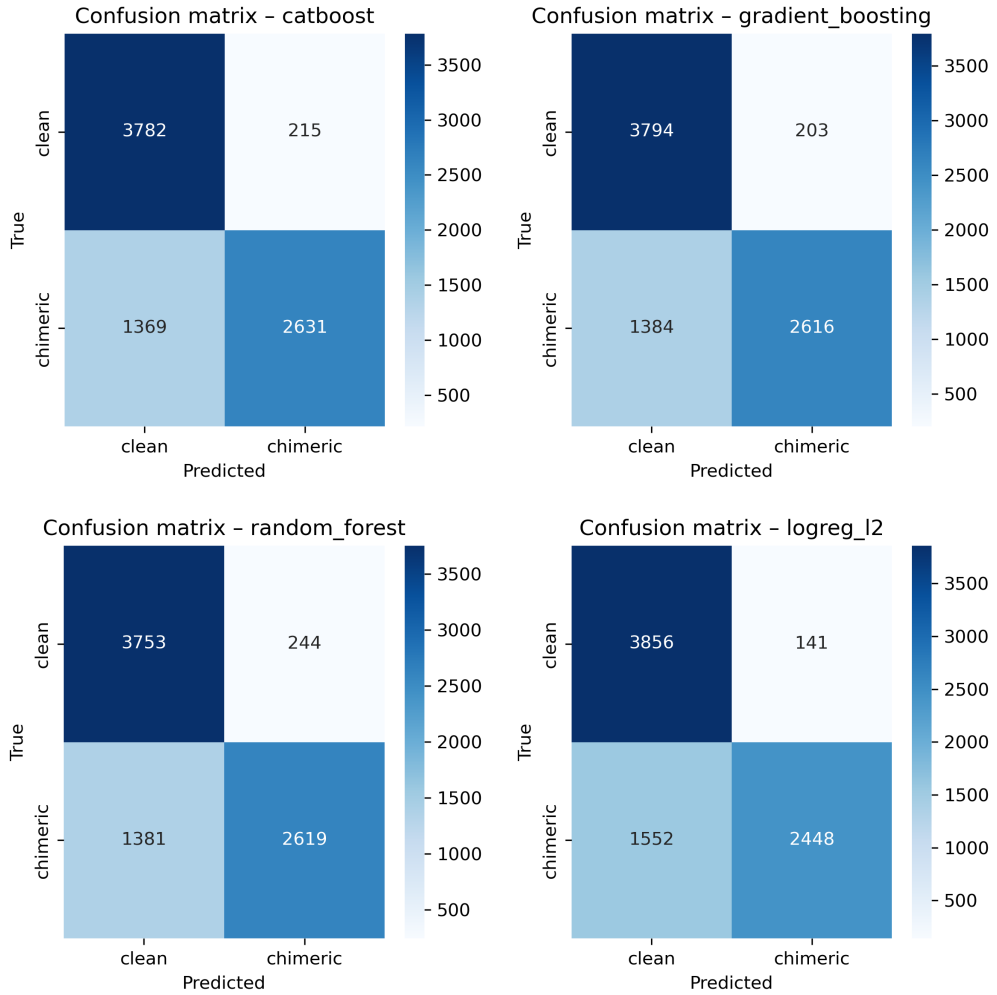


Figure 4.4: Confusion matrices for the four representative models on the held-out test set.

⁸¹⁹ 4.4.2 ROC and Precision–Recall Curves

⁸²⁰ Receiver operating characteristic (ROC) and precision–recall (PR) curves as
⁸²¹ shown in Figure 4.5 further support the similarity among the top models. The
⁸²² three tree-based ensembles (CatBoost, gradient boosting, random forest) achieved
⁸²³ ROC–AUC values of approximately 0.84 and average precision (AP) around 0.88.

824 Logistic regression performed slightly worse ($AUC \approx 0.82$, $AP \approx 0.87$) but still
825 substantially better than the dummy baseline.

826 The PR curves show that precision remains above 0.9 across a broad range
827 of recall values (up to roughly 0.5–0.6), after which precision gradually declines.
828 This behaviour indicates that the models can assign very high confidence to a
829 subset of chimeric reads, while more ambiguous reads can only be recovered by
830 accepting lower precision.

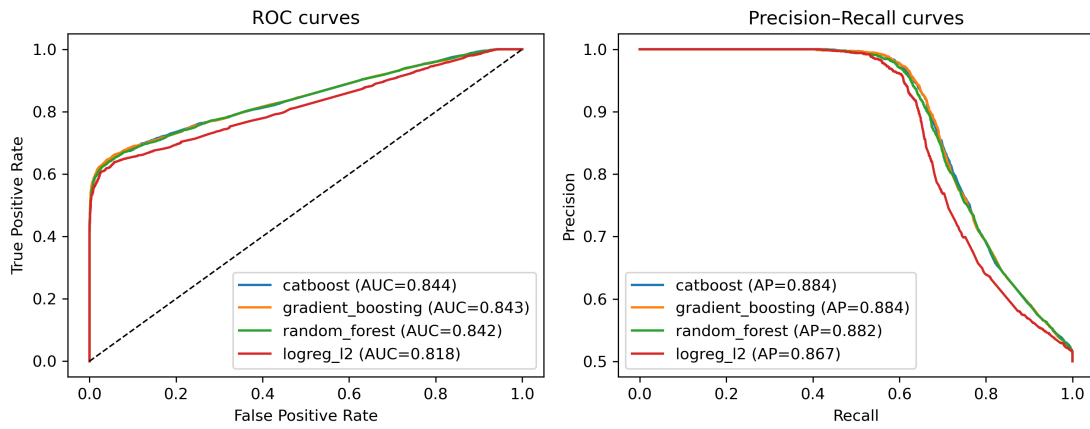


Figure 4.5: ROC (left) and precision–recall (right) curves for the four representative models on the held-out test set.

831 4.5 Feature Importance

832 4.5.1 Permutation Importance of Individual Features

833 To understand how each classifier made predictions, feature importance was quan-
834 tified using permutation importance. This analysis was applied to four represen-
835 tative models: CatBoost, Gradient Boosting, Random Forest, and L₂-regularized

836 Logistic Regression.

837 As shown in Figure 4.6, the total number of clipped bases consistently pro-
838 vides a strong predictive signal, particularly in Random Forest, Gradient Boosting,
839 and L₂-regularized Logistic Regression. CatBoost differs by assigning the highest
840 importance to k-mer divergence metrics such as `kmer_js_divergence`, which cap-
841 ture subtle sequence changes resulting from structural variants or PCR-induced
842 chimeras. Soft-clipping features (`softclip_left` and `softclip_right`) provide
843 more information around breakpoints, complementing these primary signals in all
844 models except Gradient Boosting. L₂-regularized Logistic Regression relies more
845 on alignment-based split-read metrics.

846 Overall, these results indicate that accurate detection of chimeric reads relies
847 on both alignment-based signals and k-mer compositional information. Explicit
848 microhomology features contribute minimally in this analysis, and combining both
849 alignment-based and sequence-level features enhances model sensitivity and speci-
850 ficity.

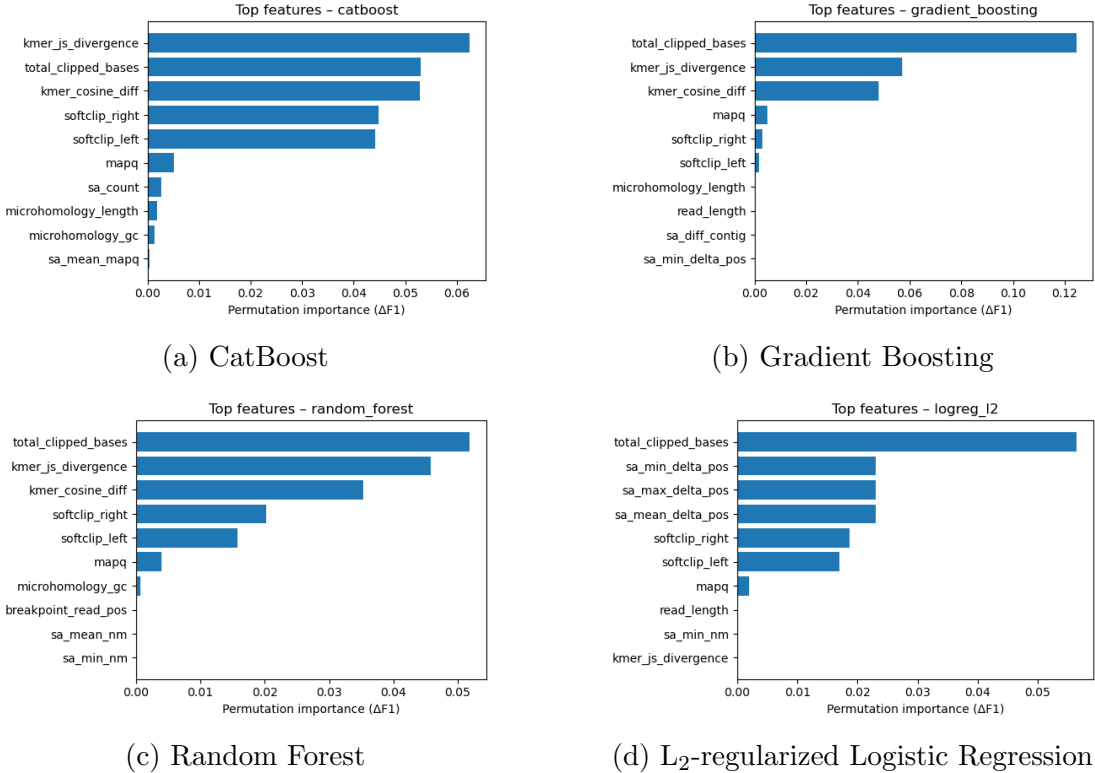


Figure 4.6: Permutation-based feature importance for four representative classifiers.

851 4.5.2 Feature Family Importance

852 To evaluate the contribution of broader signals, features were grouped into
 853 five families: SA_structure (supplementary alignment and segment met-
 854 rics, e.g., has_sa, sa_count, sa_min_delta_pos, sa_mean_nm, etc.), Clipping
 855 (softclip_left, softclip_right, total_clipped_bases, breakpoint_read_pos),
 856 Kmer_jump (kmer_cosine_diff, kmer_js_divergence), Micro_homology (microhomology_length,
 857 microhomology_gc), and Other (e.g., mapq).

858 Aggregated analyses reveal consistent patterns across models. In CatBoost,
 859 the Clipping family has the largest cumulative contribution (0.14), followed

860 by Kmer_jump (0.12), with Other features contributing minimally (0.005) and
861 SA_structure (0.003) and Micro_homology (0.003) providing minimal predictive
862 power. Gradient Boosting shows a similar trend, with Clipping (0.13) domi-
863 nating, Kmer_jump (0.11) secondary, and the remaining families contributing
864 negligibly. Random Forest integrates both Clipping (0.088) and Kmer_jump
865 (0.08) effectively, while SA_structure, Micro_homology, and Other remain minor
866 contributors. L₂-regularized Logistic Regression emphasizes Clipping (0.09)
867 and SA_structure (0.07), with Kmer_jump and Micro_homology having minimal
868 impact.

869 Both feature-level and aggregated analyses indicate that detection of chimeric
870 reads in this dataset relies primarily on alignment irregularities (Clipping) and
871 k-mer compositional shifts (Kmer_jump), which often arise from PCR-induced
872 template switching events, while explicit microhomology features contribute min-
873 imally.

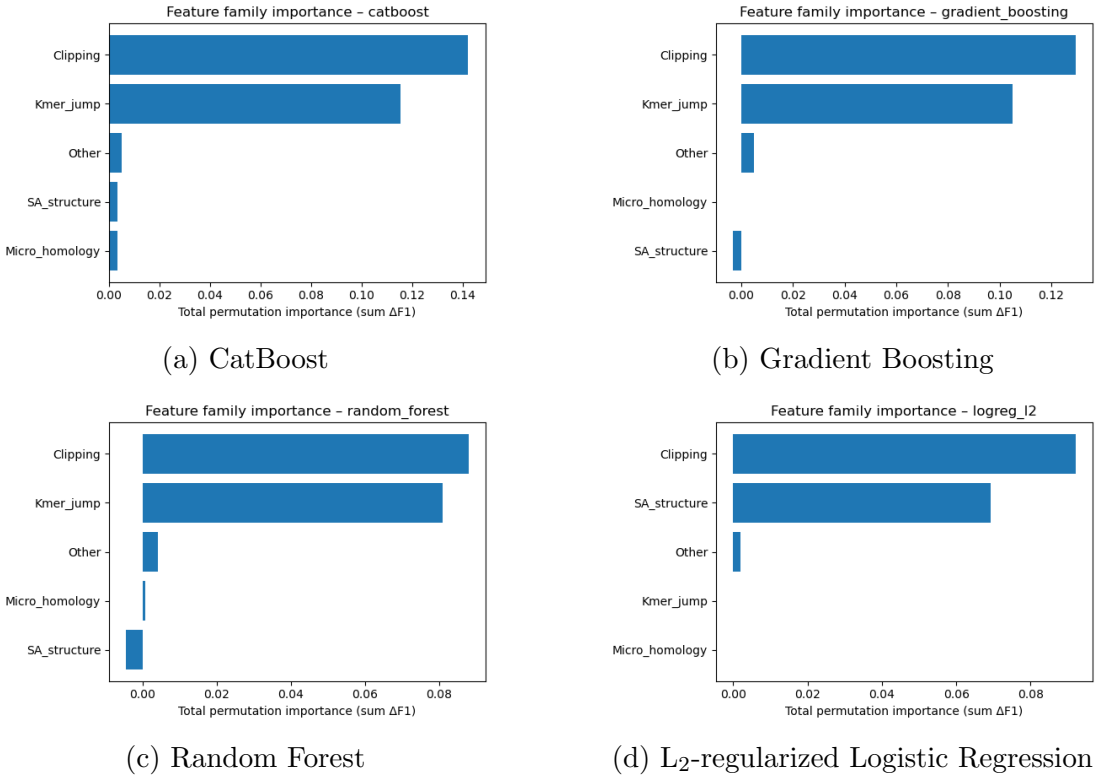


Figure 4.7: Aggregated feature family importance across four models.

874 4.6 Summary of Findings

875 All models performed substantially better than the dummy baseline, with test
 876 F1-scores around 0.76 and ROC-AUC values near 0.84. Hyperparameter tuning
 877 yielded modest improvements, with boosting methods, particularly CatBoost and
 878 gradient boosting, achieving the highest performance. Confusion matrices and
 879 precision-recall curves indicate that the models prioritize precision over recall for
 880 chimeric reads, minimizing false positives.

881 Feature importance analysis highlighted alignment breakpoints, such as clip-
 882 ping, and abrupt shifts in k-mer composition as the main contributors to predic-

883 tive power. Microhomology metrics and supplementary alignment features had
884 minimal impact. These findings suggest that alignment-based and k-mer-based
885 features alone are sufficient for training classifiers to detect mitochondrial PCR-
886 induced chimeric reads under the conditions tested.

887 **Appendix A**

888 **Exploratory Data Analysis**

889 **A.1 Histograms of Key Features**

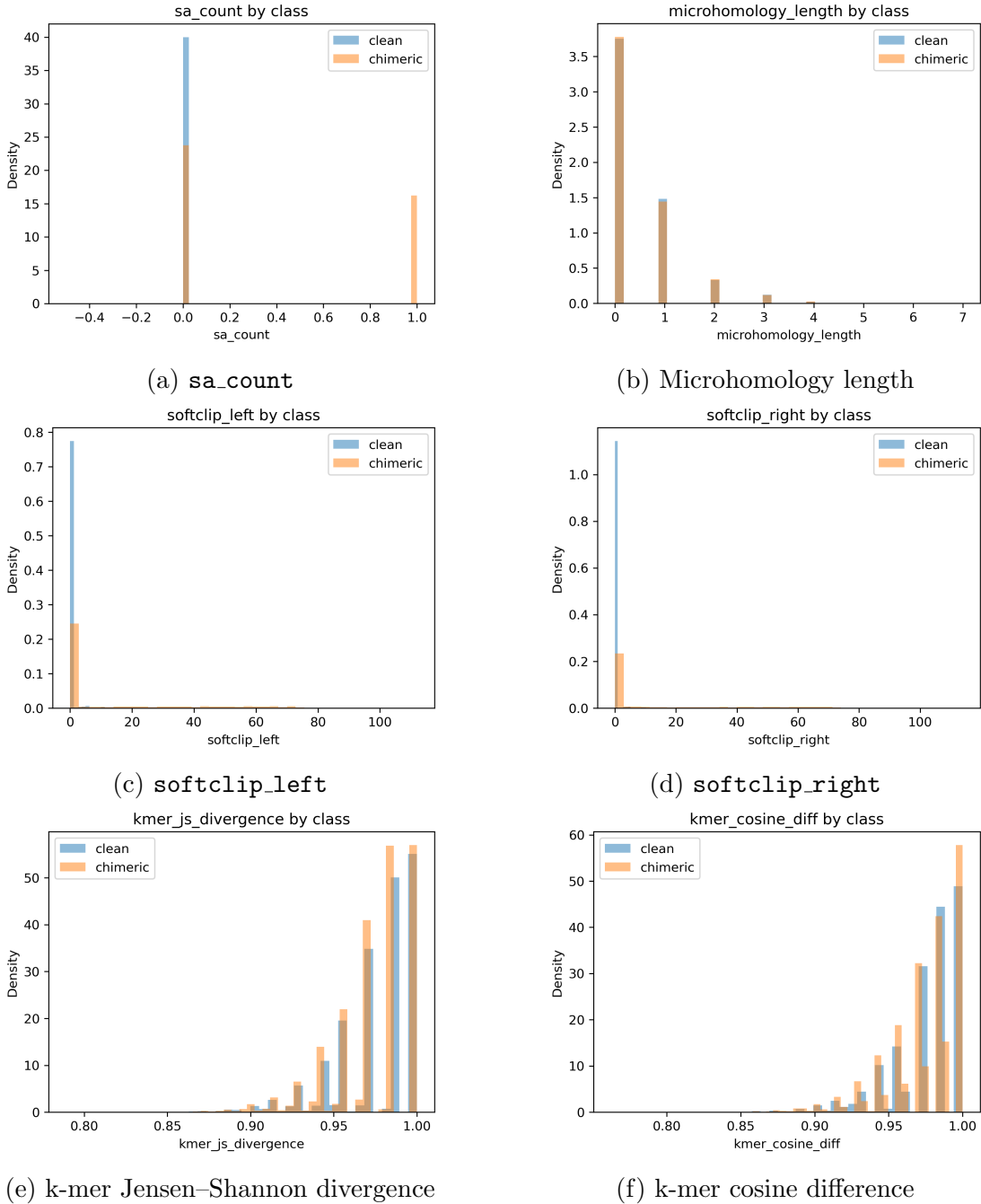


Figure A.1: Histogram plots of six key features comparing clean and chimeric reads.

890 References

- 891 Anderson, S., Bankier, A., Barrell, B., Bruijn, M., Coulson, A., Drouin, J., ...
892 Young, I. (1981, 04). Sequence and organization of the human mitochondrial
893 genome. *Nature*, *290*, 457-465. doi: 10.1038/290457a0
- 894 Arango, G., Garner, E., Pruden, A., Heath, L., Vikesland, P., & Zhang, L. (2018,
895 02). Deeparg: A deep learning approach for predicting antibiotic resistance
896 genes from metagenomic data. *Microbiome*, *6*. doi: 10.1186/s40168-018
897 -0401-z
- 898 Bentley, D. R., Balasubramanian, S., Swerdlow, H. P., Smith, G. P., Milton, J.,
899 Brown, C. G., ... Smith, A. J. (2008). Accurate whole human genome
900 sequencing using reversible terminator chemistry. *Nature*, *456*(7218), 53–
901 59. doi: 10.1038/nature07517
- 902 Boore, J. L. (1999). Animal mitochondrial genomes. *Nucleic Acids Research*,
903 *27*(8), 1767–1780. doi: 10.1093/nar/27.8.1767
- 904 Cameron, S. L. (2014). Insect mitochondrial genomics: Implications for evolution
905 and phylogeny. *Annual Review of Entomology*, *59*, 95–117. doi: 10.1146/
906 annurev-ento-011613-162007
- 907 Dierckxsens, N., Mardulyn, P., & Smits, G. (2017). Novoplasty: de novo assembly
908 of organelle genomes from whole genome data. *Nucleic Acids Research*,

- 909 45(4), e18. doi: 10.1093/nar/gkw955
- 910 Edgar, R. C. (n.d.). *Uchime in practice*. Retrieved from https://www.drive5.com/usearch/manual7/uchime_practical.html
- 911
- 912 Edgar, R. C. (2016). Uchime2: improved chimera prediction for amplicon se-
913 quencing. *bioRxiv*. Retrieved from <https://api.semanticscholar.org/>
914 CorpusID:88955007
- 915 Edgar, R. C., Haas, B. J., Clemente, J. C., Quince, C., & Knight, R. (2011).
916 Uchime improves sensitivity and speed of chimera detection. *Bioinformatics*,
917 27(16), 2194–2200. doi: 10.1093/bioinformatics/btr381
- 918 Glenn, T. C. (2011). Field guide to next-generation dna sequencers. *Molecular
919 Ecology Resources*, 11(5), 759–769. doi: 10.1111/j.1755-0998.2011.03024.x
- 920 Gonzalez, J. M., Zimmermann, J., & Saiz-Jimenez, C. (2004, 09). Evalu-
921 ating putative chimeric sequences from pcr-amplified products. *Bioin-
922 formatics*, 21(3), 333-337. Retrieved from <https://doi.org/10.1093/bioinformatics/bti008>
923 doi: 10.1093/bioinformatics/bti008
- 924 Gray, M. W. (2012). Mitochondrial evolution. *Cold Spring Harbor perspectives
925 in biology*, 4. Retrieved from <https://doi.org/10.1101/cshperspect.a011403>
926 doi: 10.1101/cshperspect.a011403
- 927 Hahn, C., Bachmann, L., & Chevreux, B. (2013). Reconstructing mitochondrial
928 genomes directly from genomic next-generation sequencing reads—a baiting
929 and iterative mapping approach. *Nucleic Acids Research*, 41(13), e129. doi:
930 10.1093/nar/gkt371
- 931 Jin, J.-J., Yu, W.-B., Yang, J., Song, Y., dePamphilis, C. W., Yi, T.-S., & Li,
932 D.-Z. (2020). Getorganelle: a fast and versatile toolkit for accurate de
933 novo assembly of organelle genomes. *Genome Biology*, 21(1), 241. doi:
934 10.1186/s13059-020-02154-5

- 935 Judo, M. S. B., Wedel, W. R., & Wilson, B. H. (1998). Stimulation and sup-
936 pression of pcr-mediated recombination. *Nucleic Acids Research*, 26(7),
937 1819–1825. doi: 10.1093/nar/26.7.1819
- 938 Labrador, K., Agmata, A., Palermo, J. D., Ravago-Gotanco, R., & Pante, M. J.
939 (2021). Mitochondrial dna reveals genetically structured haplogroups of
940 bali sardinella (sardinella lemuru) in philippine waters. *Regional Studies in*
941 *Marine Science*, 41, 101588. doi: 10.1016/j.rsma.2020.101588
- 942 Li, H. (2018, 05). Minimap2: pairwise alignment for nucleotide sequences. *Bioin-*
943 *formatics*, 34(18), 3094-3100. Retrieved from <https://doi.org/10.1093/bioinformatics/bty191>
944 doi: 10.1093/bioinformatics/bty191
- 945 Liang, Q., Bible, P. W., Liu, Y., Zou, B., & Wei, L. (2020, 02). Deepmi-
946 crobes: taxonomic classification for metagenomics with deep learning. *NAR*
947 *Genomics and Bioinformatics*, 2(1), lqaa009. Retrieved from <https://doi.org/10.1093/nargab/lqaa009> doi: 10.1093/nargab/lqaa009
- 948 Metzker, M. L. (2010). Sequencing technologies — the next generation. *Nature*
949 *Reviews Genetics*, 11(1), 31–46. doi: 10.1038/nrg2626
- 950 Mysara, M., Saeys, Y., Leys, N., Raes, J., & Monsieurs, P. (2015). Catch,
951 an ensemble classifier for chimera detection in 16s rrna sequencing stud-
952 ies. *Applied and Environmental Microbiology*, 81(5), 1573-1584. Retrieved
953 from <https://journals.asm.org/doi/abs/10.1128/aem.02896-14> doi:
954 10.1128/AEM.02896-14
- 955 Peccoud, J., Lequime, S., Moltini-Conclois, I., Giraud, I., Lambrechts, L., &
956 Gilbert, C. (2018, 04). A survey of virus recombination uncovers canon-
957 ical features of artificial chimeras generated during deep sequencing li-
958 brary preparation. *G3 Genes—Genomes—Genetics*, 8(4), 1129-1138. Re-
959 trieved from <https://doi.org/10.1534/g3.117.300468> doi: 10.1534/
960

- 961 g3.117.300468
- 962 Qin, Y., Wu, L., Zhang, Q., Wen, C., Nostrand, J. D. V., Ning, D., ... Zhou, J.
963 (2023). Effects of error, chimera, bias, and gc content on the accuracy of
964 amplicon sequencing. *mSystems*, 8(6), e01025-23. Retrieved from <https://journals.asm.org/doi/abs/10.1128/msystems.01025-23> doi: 10.1128/
965 msystems.01025-23
- 966
- 967 Qiu, X., Wu, L., Huang, H., McDonel, P. E., Palumbo, A. V., Tiedje, J. M., &
968 Zhou, J. (2001). Evaluation of pcr-generated chimeras, mutations, and het-
969 eroduplexes with 16s rrna gene-based cloning. *Applied and Environmental*
970 *Microbiology*, 67(2), 880–887. doi: 10.1128/AEM.67.2.880-887.2001
- 971 Ren, J., Song, K., Deng, C., Ahlgren, N., Fuhrman, J., Li, Y., ... Sun, F. (2020,
972 01). Identifying viruses from metagenomic data using deep learning. *Quan-*
973 *titative Biology*, 8. doi: 10.1007/s40484-019-0187-4
- 974 Rodriguez-Martin, B., Palumbo, E., Marco-Sola, S., Griebel, T., Ribeca, P.,
975 Alonso, G., ... Djebali, S. (2017, 01). Chimpipe: Accurate detection of
976 fusion genes and transcription-induced chimeras from rna-seq data. *BMC*
977 *Genomics*, 18. doi: 10.1186/s12864-016-3404-9
- 978 Rognes, T., Flouri, T., Nichols, B., Quince, C., & Mahé, F. (2016). Vsearch: a
979 versatile open source tool for metagenomics. *PeerJ*, 4, e2584. doi: 10.7717/
980 peerj.2584
- 981 Sedlazeck, F., Rescheneder, P., Smolka, M., Fang, H., Nattestad, M., von Haeseler,
982 A., & Schatz, M. (2018, 06). Accurate detection of complex structural
983 variations using single-molecule sequencing. *Nature Methods*, 15. doi: 10
984 .1038/s41592-018-0001-7
- 985 Sfeir, A., & Symington, L. S. (2015). Microhomology-mediated end joining: A
986 back-up survival mechanism or dedicated pathway? *Trends in Biochemical*

- 987 *Sciences*, 40(11), 701-714. Retrieved from <https://www.sciencedirect.com/science/article/pii/S0968000415001589> doi: <https://doi.org/10.1016/j.tibs.2015.08.006>
- 988
- 989
- 990 Vervier, K., Mahé, P., Tournoud, M., Veyrieras, J.-B., & Vert, J.-P. (2015,
- 991 11). Large-scale machine learning for metagenomics sequence classifica-
- 992 tion. *Bioinformatics*, 32(7), 1023-1032. Retrieved from <https://doi.org/10.1093/bioinformatics/btv683> doi: 10.1093/bioinformatics/btv683
- 993
- 994 Willette, D., Bognot, E., Mutia, M. T., & Santos, M. (2011). *Biology and ecology*
- 995 of sardines in the philippines: A review (Vol. 13; Tech. Rep. No. 1). NFRDI
- 996 Technical Paper Series. Retrieved from <https://nfrdi.da.gov.ph/tpjf/etc/Willette%20et%20al.%20Sardines%20Review.pdf>
- 997